

A stable finite difference method for the elastic wave equation on complex geometries with free surfaces

Daniel Appelö^{1,*} and N. Anders Petersson²

¹ *Department of Mechanical Engineering, California Institute of Technology, Pasadena, CA 91125, USA*

² *Center for Applied and Scientific Computing, Lawrence Livermore National Laboratory, Livermore, CA 94551, USA*

Abstract. A stable and explicit second order accurate finite difference method for the elastic wave equation in curvilinear coordinates is presented. The discretization of the spatial operators in the method is shown to be selfadjoint for free-surface, Dirichlet and periodic boundary conditions. The fully discrete version of the method conserves a discrete energy to machine precision.

AMS subject classifications: 65M06, 74B05, 86A15

Key words: elastic wave equation; curvilinear grids ; finite differences; stability; energy estimate; seismic wave propagation

1 Introduction

The isotropic elastic wave equation governs the propagation of seismic waves caused by earthquakes and other seismic events. It also governs the propagation of waves in solid material structures and devices, such as gas pipes, wave guides, railroad rails and disc brakes. In the vast majority of wave propagation problems arising in seismology and solid mechanics there are free surfaces, i.e. boundaries with vanishing normal stresses. These free surfaces have, in general, complicated shapes and are rarely flat.

Another feature, characterizing problems arising in these areas, is the strong heterogeneity of the media, in which the problems are posed. For example, on the characteristic length scales of seismological problems, the geological structures of the earth can be described by piecewise smooth functions with jump discontinuities. However, compared to the wavelengths, which can be resolved in computations, the material properties vary rapidly. Large spatial contrasts are also found in solid mechanics devices composed of different materials welded together.

*Corresponding author. *Email addresses:* appel@caltech.edu (D. Appelö), andersp@llnl.gov (N. A. Petersson)

The presence of curved free surfaces, together with the typical strong material heterogeneity, makes the design of stable, efficient and accurate numerical methods for the elastic wave equation challenging. Today, many different classes of numerical methods are used for the simulation of elastic waves. Early on, most of the methods were based on finite difference approximations of space and time derivatives of the equations in second order differential form (displacement formulation), see for example [1, 2]. The main problem with these early discretizations were their inability to approximate free surface boundary conditions in a stable and fully explicit manner, see e.g. [10, 11, 18, 21]. The instabilities of these early methods were especially bad for problems with materials with high ratios between the P-wave (C_p) and S-wave (C_s) velocities.

For rectangular domains, a stable and explicit discretization of the free surface boundary conditions is presented in the paper [17] by Nilsson et al. In summary, they introduce a discretization that use boundary-modified difference operators for the mixed derivatives in the governing equations. Nilsson et al. show that the method is second order accurate for problems with smoothly varying material properties and stable under standard CFL constraints, for *arbitrarily* varying material properties.

In this paper we generalize the results of Nilsson et al. to curvilinear coordinate systems, allowing for simulations on non-rectangular domains. Using summation by parts techniques, we show how to construct a corresponding stable discretization of the free surface boundary condition on curvilinear grids. We also prove that the discretization is stable and energy conserving both in semi-discrete and fully discrete form. As for the Cartesian method in [17], the stability and conservation results holds for *arbitrarily varying material properties*. By numerical experiments it is established that the method is second order accurate.

The strengths of the proposed method are its ease of implementation, its (relative to low order unstructured grid methods) efficiency, its geometric flexibility, and, most importantly, its "bullet-proof" stability. The proposed method is second order accurate for materials with smoothly varying properties. However, it has been known for a long time [14] that second order methods are less efficient than higher (4th or more) order methods. When the material properties are only piecewise smooth (as e.g. in seismology), the difference in efficiency between high and low order accurate methods is not as pronounced, see e.g. [4, 9]. For such problems the formal order of accuracy (for both high and low order methods) is reduced to one, but as has been shown in [4], the higher order methods produce more accurate results. Although we believe that the present method is reasonably competitive for strongly heterogeneous materials, it would be of great interest to derive a similarly "bullet-proof" fourth or higher order accurate method.

There are of course many other numerical methods capable of handling general geometries. Two recent finite difference methods are the traction image method for curvilinear grids [22], and the embedded boundary method by Lombard et al. described in [15]. Both these methods use dissipative time-integration schemes while our method is non-dissipative and energy conserving. In comparison to the embedded boundary method of Lombard et al., our method works best for problems where most of the computations

take place close to a surface (where an embedded boundary method has large overhead), while the embedded boundary method is more efficient for problems with large volume to surface ratio. Regarding the stability of the methods in [15, 22], no theoretical results are provided in the papers (in the latter paper stability is tested in a long-time simulation).

Other methods include the well-established spectral element method [7, 13, 20], the pseudospectral method [8] and the discontinuous Galerkin method [12]. For homogeneous materials these methods can, in principle, be made arbitrary accurate as the order n of the polynomial approximation increases. This property together with the geometrical flexibility of unstructured methods make spectral element and discontinuous Galerkin methods attractive for simulation of elastic waves in complex geometries. A drawback of spectral elements, pseudospectral methods and discontinuous Galerkin methods is that the maximum time step (when an explicit time stepping method is used) decrease as $1/n$, thus when the order of the polynomial approximation go up the time step becomes smaller. In addition, to fully utilize the high order approximations, the unstructured grids must be of high quality. The construction of such high quality grids, based on quad/hex elements, can be labor intensive and is not easily automated. As for finite difference methods, the formal order of these methods will be reduced to first order if material discontinuities are not aligned with element boundaries, see [6, 9].

The rest of the paper is organized as follows: In §2 we state the governing equations and boundary conditions in Cartesian and curvilinear coordinates. In §3 we introduce the proposed numerical method, and prove several results concerning its stability and conservation properties. Both the semi-discrete and fully discretized versions of the method are discussed. We also comment on how to extend the method to three dimensions. In §4 we give several numerical examples in two and three dimensions. We verify the order of the method for smooth materials and its discrete conservation properties for arbitrarily varying materials. Finally, in §5 we summarize and conclude.

2 The governing equations

Consider the propagation of elastic waves in a non-rectangular domain like the one depicted to the left in Figure 1. In a Cartesian coordinate system (the $x-y$ system to the left in Figure 1) the elastic wave equation, without external forcing, takes the form

$$\rho \frac{\partial^2 u}{\partial t^2} = \frac{\partial}{\partial x} \left((2\mu + \lambda) \frac{\partial}{\partial x} u + \lambda \frac{\partial}{\partial y} v \right) + \frac{\partial}{\partial y} \left(\mu \left(\frac{\partial}{\partial x} v + \frac{\partial}{\partial y} u \right) \right), \quad (2.1)$$

$$\rho \frac{\partial^2 v}{\partial t^2} = \frac{\partial}{\partial x} \left(\mu \left(\frac{\partial}{\partial x} v + \frac{\partial}{\partial y} u \right) \right) + \frac{\partial}{\partial y} \left(\lambda \frac{\partial}{\partial x} u + (2\mu + \lambda) \frac{\partial}{\partial y} v \right). \quad (2.2)$$

Here u and v are the displacements in the x and y directions. The Lamé parameters, $\mu = \mu(x, y)$, $\lambda = \lambda(x, y)$ and the density $\rho = \rho(x, y)$, are restricted to be real valued positive

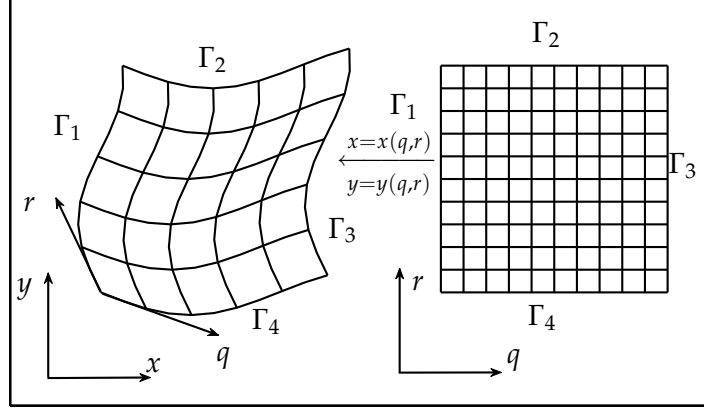


Figure 1: The mapping between physical (left) and computational coordinates (right). The free surface on the left is mapped onto $q=0$ and the lower boundary is mapped onto $r=0$.

functions, but are allowed to vary arbitrarily in space. The equations (2.1) - (2.2) are augmented by the initial data

$$\begin{aligned} u(x,y,0) &= u_0(x,y), & v(x,y,0) &= v_0(x,y), \\ \frac{\partial u(x,y,0)}{\partial t} &= u_1(x,y), & \frac{\partial v(x,y,0)}{\partial t} &= v_1(x,y). \end{aligned}$$

In this paper we consider three types of boundary conditions: free surface, Dirichlet and periodic boundary conditions. For simplicity, we first describe a case where only side Γ_1 (where $q=0$) is a free surface; later on (see §3.4) we outline how to discretize cases where two or more free surfaces are present.

On the free surface Γ_1 we impose the boundary conditions

$$\begin{bmatrix} (2\mu + \lambda) \frac{\partial u}{\partial x} + \lambda \frac{\partial v}{\partial y} & \mu \left(\frac{\partial v}{\partial x} + \frac{\partial u}{\partial y} \right) \\ \mu \left(\frac{\partial v}{\partial x} + \frac{\partial u}{\partial y} \right) & (2\mu + \lambda) \frac{\partial v}{\partial y} + \lambda \frac{\partial u}{\partial x} \end{bmatrix} \begin{bmatrix} n_x \\ n_y \end{bmatrix} = 0. \quad (2.3)$$

Here $[n_x, n_y]^T$ is the inward normal of Γ_1 . On the sides Γ_2, Γ_4 we impose periodic boundary conditions and on Γ_3 we impose homogeneous Dirichlet boundary conditions

$$u|_{\Gamma_3} = v|_{\Gamma_3} = 0. \quad (2.4)$$

2.1 The elastic wave equation in a curvilinear coordinate system

Before we discretize the governing equations and the boundary conditions we transform them to a curvilinear coordinate system that conforms with the boundaries of the domain,

see Figure 1.

Assume that there is a one to one mapping

$$x = x(q, r), \quad y = y(q, r), \quad (q, r) \in [0, 1]^2,$$

from the unit square to the domain confined by $\Gamma_1, \Gamma_2, \Gamma_3, \Gamma_4$. By the chain rule we have the relations

$$\partial_x = q_x \partial_q + r_x \partial_r, \quad \partial_y = q_y \partial_q + r_y \partial_r, \quad \partial_q = x_q \partial_x + y_q \partial_y, \quad \partial_r = x_r \partial_x + y_r \partial_y, \quad (2.5)$$

where q_x denotes $\frac{\partial q(x, y)}{\partial x}$ etc. and are referred to as metric derivatives or simply the metric. After inverting (2.5) we find the metric derivatives

$$\begin{bmatrix} q_x & r_x \\ q_y & r_y \end{bmatrix} = \frac{1}{J} \begin{bmatrix} y_r & -y_q \\ -x_r & x_q \end{bmatrix},$$

where $J = x_q y_r - x_r y_q$ is the Jacobian of the mapping.

Utilizing (2.5) the equations (2.1) and (2.2) are transformed into (for details see e.g [19])

$$\begin{aligned} J\rho \frac{\partial^2 u}{\partial t^2} = & \frac{\partial}{\partial q} \left[Jq_x \left[(2\mu + \lambda) (q_x \partial_q + r_x \partial_r) u + \lambda (q_y \partial_q + r_y \partial_r) v \right] \right. \\ & \left. + Jq_y \left[\mu \left((q_x \partial_q + r_x \partial_r) v + (q_y \partial_q + r_y \partial_r) u \right) \right] \right] \\ & + \frac{\partial}{\partial r} \left[Jr_x \left[(2\mu + \lambda) (q_x \partial_q + r_x \partial_r) u + \lambda (q_y \partial_q + r_y \partial_r) v \right] \right. \\ & \left. + Jr_y \left[\mu \left((q_x \partial_q + r_x \partial_r) v + (q_y \partial_q + r_y \partial_r) u \right) \right] \right], \quad (2.6) \end{aligned}$$

$$\begin{aligned} J\rho \frac{\partial^2 v}{\partial t^2} = & \frac{\partial}{\partial q} \left[Jq_x \left[\mu \left((q_x \partial_q + r_x \partial_r) v + (q_y \partial_q + r_y \partial_r) u \right) \right] \right. \\ & \left. + Jq_y \left[(2\mu + \lambda) (q_y \partial_q + r_y \partial_r) v + \lambda (q_x \partial_q + r_x \partial_r) u \right] \right] \\ & + \frac{\partial}{\partial r} \left[Jr_x \left[\mu \left((q_x \partial_q + r_x \partial_r) v + (q_y \partial_q + r_y \partial_r) u \right) \right] \right. \\ & \left. + Jr_y \left[(2\mu + \lambda) (q_y \partial_q + r_y \partial_r) v + \lambda (q_x \partial_q + r_x \partial_r) u \right] \right]. \quad (2.7) \end{aligned}$$

Similarly, the free surface boundary conditions are transformed into

$$\bar{q}_x \left[(2\mu + \lambda) (q_x u_q + r_x u_r) + \lambda (q_y v_q + r_y v_r) \right] + \bar{q}_y \mu \left((q_x v_q + r_x v_r) + (q_y u_q + r_y u_r) \right) = 0, \quad (2.8)$$

$$\bar{q}_x \mu \left((q_x v_q + r_x v_r) + (q_y u_q + r_y u_r) \right) + \bar{q}_y \left[(2\mu + \lambda) (q_x v_q + r_x v_r) + \lambda (q_y u_q + r_y u_r) \right] = 0. \quad (2.9)$$

Note that here the normal is represented by the normalized metric (evaluated along $q=0$)

$$\bar{q}_x = \frac{q_x}{\sqrt{q_x^2 + q_y^2}}, \quad \bar{q}_y = \frac{q_y}{\sqrt{q_x^2 + q_y^2}}.$$

3 A self-adjoint discretization of the elastic wave equation on a curvilinear grid

To approximate (2.6) and (2.7) we cover the unit square with the grid

$$\begin{aligned} q_i &= (i-1)h_q, \quad i=0, \dots, N_q, \quad h_q = 1/(N_q-1), \\ r_j &= (j-1)h_r, \quad j=0, \dots, N_r+1, \quad h_r = 1/(N_r-1). \end{aligned}$$

Here the grid indexes $(i, j) \in [1, N_q-1] \times [1, N_r]$ belong to interior points where (2.1), (2.2) are approximated and the rest belong to points that are assigned by enforcing the boundary conditions. On this grid we introduce the real valued grid functions $[u_{i,j}(t), v_{i,j}(t)] = [u(q_i, r_j, t), v(q_i, r_j, t)]$ and the standard difference operators

$$\begin{aligned} D_+^q u_{i,j} &= \frac{u_{i+1,j} - u_{i,j}}{h_q}, \quad D_-^q u_{i,j} = D_+^q u_{i-1,j}, \\ D_+^r u_{i,j} &= \frac{u_{i,j+1} - u_{i,j}}{h_r}, \quad D_-^r u_{i,j} = D_+^r u_{i,j-1}, \\ D_0^q u_{i,j} &= \frac{1}{2}(D_+^q u_{i,j} + D_-^q u_{i,j}), \quad D_0^r u_{i,j} = \frac{1}{2}(D_+^r u_{i,j} + D_-^r u_{i,j}), \end{aligned}$$

as well as the boundary modified operator

$$\widetilde{D}_0^q u_{i,j} = \begin{cases} D_+^q u_{i,j}, & i=1, \\ D_0^q u_{i,j}, & i \geq 2. \end{cases}$$

We also introduce the averaging operators

$$E_{1/2}^q(\sigma_{i,j}) = \frac{1}{2}(\sigma_{i+1,j} + \sigma_{i,j}), \quad E_{1/2}^r(\sigma_{i,j}) = \frac{1}{2}(\sigma_{i,j+1} + \sigma_{i,j}).$$

3.1 The spatial discretization

The right hand sides of (2.6), (2.7) contain spatial derivatives of four basic types, which are discretized according to

$$\frac{\partial}{\partial q}(aw_q) \approx D_-^q \left(E_{1/2}^q(a) D_+^q w \right), \quad \frac{\partial}{\partial q}(bw_r) \approx \widetilde{D}_0^q (b D_0^r w), \quad (3.1)$$

$$\frac{\partial}{\partial r}(cw_q) \approx D_0^r \left(c \widetilde{D}_0^q w \right), \quad \frac{\partial}{\partial r}(dw_r) \approx D_-^r \left(E_{1/2}^r(d) D_+^r w \right). \quad (3.2)$$

Here w represents either u or v , and a , b , c , and d are combinations of metric and material coefficients.

To cast the discretized equations in a more compact form, we introduce the following notation for the material and metric terms,

$$\begin{aligned} M_1^{kl} &= Jk_x l_x (2\mu + \lambda) + Jk_y l_y \mu, \\ M_2^{kl} &= Jk_x l_y \lambda + Jk_y l_x \mu, \\ M_3^{kl} &= Jk_y l_y (2\mu + \lambda) + Jk_x l_x \mu, \end{aligned}$$

where k and l represent the metric coefficients q or r . We approximate the spatial operators in equations (2.6) and (2.7) by the approximations (3.1) and (3.2). After the grid indexes have been suppressed to improve readability, this leads to

$$\begin{aligned} J\rho \frac{\partial^2 u}{\partial t^2} &= D_-^q \left(E_{1/2}^q (M_1^{qq}) D_+^q u + E_{1/2}^q (M_2^{qq}) D_+^q v \right) + \widetilde{D}_0^q \left(M_1^{qr} D_0^r u + M_2^{qr} D_0^r v \right) \\ &+ D_0^r \left(M_1^{rq} \widetilde{D}_0^q u + M_2^{rq} \widetilde{D}_0^q v \right) + D_-^r \left(E_{1/2}^r (M_1^{rr}) D_+^r u + E_{1/2}^r (M_2^{rr}) D_+^r v \right) \equiv L^{(u)}(u, v), \end{aligned} \quad (3.3)$$

$$\begin{aligned} J\rho \frac{\partial^2 v}{\partial t^2} &= D_-^q \left(E_{1/2}^q (M_3^{qq}) D_+^q v + E_{1/2}^q (M_2^{qq}) D_+^q u \right) + \widetilde{D}_0^q \left(M_3^{qr} D_0^r v + M_2^{qr} D_0^r u \right) \\ &+ D_0^r \left(M_3^{rq} \widetilde{D}_0^q v + M_2^{rq} \widetilde{D}_0^q u \right) + D_-^r \left(D_-^r E_{1/2}^r (M_3^{rr}) D_+^r v + E_{1/2}^r (M_2^{rr}) D_+^r u \right) \equiv L^{(v)}(u, v), \end{aligned} \quad (3.4)$$

in the grid points $(q_i, r_j), (i, j) \in [1, N_q - 1] \times [1, N_r]$. The discrete boundary conditions corresponding to (2.4) are

$$\left. \begin{aligned} u_{N_q, j} &= 0 \\ v_{N_q, j} &= 0 \end{aligned} \right\} j = 1, \dots, N_r, \quad (3.5)$$

and the periodic boundary conditions are $w_{i, j} = w_{i, j + N_r}, w = \{u, v\}$ which can be used to specify

$$\left. \begin{aligned} u_{i, 0} &= u_{i, N_r}, \quad u_{i, N_r + 1} = u_{i, 1}, \\ v_{i, 0} &= v_{i, N_r}, \quad v_{i, N_r + 1} = v_{i, 1}, \end{aligned} \right\} i = 0, \dots, N_q, \quad (3.6)$$

Finally, as we are about to show, a stable second order accurate approximation of the free surface boundary conditions (2.8), (2.9) is obtained by a centered approximation,

$$\begin{aligned} \frac{1}{2} \left((M_1^{qq})_{3/2, j} D_+^q u_{1, j} + (M_1^{qq})_{1/2, j} D_+^q u_{0, j} \right) + (M_1^{qr})_{1, j} D_0^r u_{1, j} \\ + \frac{1}{2} \left((M_2^{qq})_{3/2, j} D_+^q v_{1, j} + (M_2^{qq})_{1/2, j} D_+^q v_{0, j} \right) + (M_2^{qr})_{1, j} D_0^r v_{1, j} = 0, \end{aligned} \quad (3.7)$$

$$\begin{aligned} \frac{1}{2} \left((M_3^{qq})_{3/2, j} D_+^q v_{1, j} + (M_3^{qq})_{1/2, j} D_+^q v_{0, j} \right) + (M_3^{qr})_{1, j} D_0^r v_{1, j} \\ + \frac{1}{2} \left((M_2^{qq})_{3/2, j} D_+^q u_{1, j} + (M_2^{qq})_{1/2, j} D_+^q u_{0, j} \right) + (M_2^{qr})_{1, j} D_0^r u_{1, j} = 0, \end{aligned} \quad (3.8)$$

for $j = 1, \dots, N_r$.

Remark 1. The key ingredient in obtaining a stable self-adjoint *explicit* discretization is to use the operator \widetilde{D}_0^q (which is one-sided on the boundary) for the approximation of the normal derivative in the $\partial_q \partial_r$ and $\partial_r \partial_q$ cross derivatives. At first, it might appear that by using a one-sided operator the accuracy of the method would be reduced to first order. However, as was theoretically shown in [17] (for a Cartesian discretization), a first order error on the boundary in the differential equation (3.3), (3.4) can be absorbed as a second order perturbation of the boundary conditions (3.7), (3.8).

Remark 2. The above discretization does not depend on how the metric derivatives are evaluated. If the mapping is known explicitly they can be computed analytically, if not they can be computed numerically. In all numerical examples presented in this paper the metric derivatives are computed numerically using second order accurate finite difference approximations.

3.2 Some lemmata about the discretization

In this subsection we state and prove the main properties of the discretization. We begin by defining a suitable discrete inner product. Let w and u be real valued grid functions and $(w, u)_h$ be the discrete inner product

$$(w, u)_h = h_q h_r \sum_{j=1}^{N_r} \left(\frac{1}{2} w_{1,j} u_{1,j} + \sum_{i=2}^{N_q} w_{i,j} u_{i,j} \right),$$

with corresponding norm $\|w\|_h^2 = (w, w)_h$. For the present discretization we have.

Lemma 1 (Self adjointness of the spatial discretization). For all real-valued grid functions (u^0, v^0) , (u^1, v^1) satisfying the discrete boundary conditions (3.5), (3.6), (3.7), (3.8), the spatial operator $(L^{(u)}, L^{(v)})$ is self-adjoint, i.e.

$$(u^0, L^{(u)}(u^1, v^1))_h + (v^0, L^{(v)}(u^1, v^1))_h = (u^1, L^{(u)}(u^0, v^0))_h + (v^1, L^{(v)}(u^0, v^0))_h. \quad (3.9)$$

Proof. Our first step is to study the boundary contributions from $(u^0, L^{(u)}(u^1, v^1))_h$ by using the following summation by part identities:

$$\begin{aligned} (D_+^r w, u)_h + (w, D_-^r u)_h &= 0, \\ (D_0^r w, u)_h + (w, D_0^r u)_h &= 0, \\ (w, D_+^q u)_h + (D_-^q w, u)_h &= -\frac{h_r}{2} \sum_{j=1}^{N_r-1} (w_{0,j} u_{1,j} + w_{1,j} u_{2,j}) + h_r \sum_{j=1}^{N_r} w_{N_q-1,j} u_{N_q,j}, \\ (w, \widetilde{D}_0^q u)_h + (\widetilde{D}_0^q w, u)_h &= -h_r \sum_{j=1}^{N_r} w_{1,j} u_{1,j} + \frac{h_r}{2} \sum_{j=1}^{N_r} (w_{N_q,j} u_{N_q-1,j} + w_{N_q-1,j} u_{N_q,j}). \end{aligned} \quad (3.10)$$

We illustrate the ideas of the proof on the first two terms the inner product $(u^0, L^{(u)}(u^1, v^1))_h$. Starting with the first $\partial_q \partial_q$ term, $D_-^q E_{1/2}^q (Jq_x q_x (2\mu + \lambda)) D_+^q u$, we apply the above summation by parts identities and find

$$(u^0, D_-^q E_{1/2}^q (Jq_x q_x (2\mu + \lambda)) D_+^q u^1) = -(D_+^q u^0, E_{1/2}^q (Jq_x q_x (2\mu + \lambda)) D_+^q u^1) + A_1 + B_1,$$

where

$$A_1 = h_r \sum_{j=1}^{N_r} u_{N_q, j}^0 (Jq_x q_x (2\mu + \lambda))_{N_q - 1/2, j} D_+^q u_{N_q - 1, j}^1,$$

$$B_1 = -\frac{h_r}{2} \sum_{j=1}^{N_r} \left(u_{2, j}^0 (Jq_x q_x (2\mu + \lambda))_{3/2, j} D_+^q u_{1, j}^1 + u_{1, j}^0 (Jq_x q_x (2\mu + \lambda))_{1/2, j} D_+^q u_{0, j}^1 \right).$$

The homogeneous Dirichlet boundary condition on Γ_3 is $u_{N_q, j}^0 = 0$; thus the term A_1 vanishes, leaving only the boundary contribution B_1 . To get an expression for B_1 where $u_{1, j}^0$ multiplies the terms containing D_+^q (which is an approximation of the $q_x(2\mu + \lambda)u_q$ part of the boundary condition) we use the identity $u_{2, j}^0 = u_{1, j}^0 + h_q D_+^q u_{1, j}^0$ and obtain

$$B_1 = \mathfrak{B}_1(u^0, u^1, v^0, v^1) + b_1,$$

where

$$\mathfrak{B}_1(u^0, u^1, v^0, v^1) = -\frac{h_r}{2} \sum_{j=1}^{N_r} u_{1, j}^0 \left((Jq_x q_x (2\mu + \lambda))_{3/2, j} D_+^q u_{1, j}^1 + (Jq_x q_x (2\mu + \lambda))_{1/2, j} D_+^q u_{0, j}^1 \right),$$

$$b_1 = -\frac{h_r h_q}{2} \sum_{j=1}^{N_r} D_+^q u_{1, j}^0 (Jq_x q_x (2\mu + \lambda))_{3/2, j} D_+^q u_{1, j}^1.$$

The term b_1 is symmetric in u^0, u^1 and there is an identical contribution, canceling b_1 , from the first term in $(u^1, L^{(u)}(u^0, v^0))_h$.

For the second term, $\widetilde{D}_0^q (Jq_x r_x (2\mu + \lambda)) D_0^r u^1$, in $(u^0, L^{(u)}(u^1, v^1))_h$ the above identities are used again to obtain

$$(u^0, \widetilde{D}_0^q (Jq_x r_x (2\mu + \lambda)) D_0^r u^1) = -(\widetilde{D}_0^q u^0, (Jq_x r_x (2\mu + \lambda)) D_0^r u^1) + A_2 + \mathfrak{B}_2(u^0, u^1, v^0, v^1),$$

where

$$A_2 = \frac{h_r}{2} \sum_{j=1}^{N_r} (u_{N_q - 1, j}^0 (Jq_x r_x (2\mu + \lambda))_{N_q, j} D_0^r u_{N_q, j}^1 + u_{N_q, j}^0 (Jq_x r_x (2\mu + \lambda))_{N_q + 1, j} D_0^r u_{N_q - 1, j}^1),$$

$$\mathfrak{B}_2(u^0, u^1, v^0, v^1) = -h_r \sum_{j=1}^{N_r} u_{1, j}^0 \left((Jq_x r_x (2\mu + \lambda))_{1, j} D_0^r u_{1, j}^1 \right).$$

We note that $u_{N_q,j}^1 = 0$ implies $D_0^r u_{N_q,j}^1 = 0$ and thus the boundary term A_2 vanishes.

The six remaining of the first eight terms in $(u^0, L^{(u)}(u^1, v^1))_h$ gives the same type of contributions and the last eight terms will not give any boundary contributions because of the periodicity in the r direction.

Repeating the above steps for $(u^1, L^{(u)}(u^0, v^0))_h$ give the same kind of boundary terms (the arguments of \mathfrak{B}_k are ordered differently, namely $\mathfrak{B}_k(u^1, u^0, v^1, v^0)$). From $(v^0, L^{(v)}(u^1, v^1))_h$ and $(v^1, L^{(v)}(u^0, v^0))_h$ there will also be boundary terms, which we denote $\mathfrak{C}_k(u^0, u^1, v^0, v^1)$ and $\mathfrak{C}_k(u^1, u^0, v^1, v^0)$ respectively. Subtracting the right hand side of equation (3.9) from its left hand side results in the equality

$$\begin{aligned} & (u^0, L^{(u)}(u^1, v^1))_h - (u^1, L^{(u)}(u^0, v^0))_h + (v^0, L^{(v)}(u^1, v^1))_h - (v^1, L^{(v)}(u^0, v^0))_h = \\ & \sum_{k=1}^8 \mathfrak{B}_k(u^0, u^1, v^0, v^1) - \sum_{k=1}^8 \mathfrak{B}_k(u^1, u^0, v^1, v^0) + \sum_{k=1}^8 \mathfrak{C}_k(u^0, u^1, v^0, v^1) - \sum_{k=1}^8 \mathfrak{C}_k(u^1, u^0, v^1, v^0). \end{aligned} \quad (3.11)$$

The first sum on the right hand of (3.11) side equals

$$\begin{aligned} \sum_{k=1}^8 \mathfrak{B}_k(u^0, u^1, v^0, v^1) = & - \sum_{j=1}^{N_r} u_{1,j}^0 \left[\frac{1}{2} \left((M_1^{qq})_{3/2,j} D_+^q u_{1,j} + (M_1^{qq})_{1/2,j} D_+^q u_{0,j} \right) + (M_1^{qr})_{1,j} D_0^r u_{1,j} \right. \\ & \left. + \frac{1}{2} \left((M_2^{qq})_{3/2,j} D_+^q v_{1,j} + (M_2^{qq})_{1/2,j} D_+^q v_{0,j} \right) + (M_2^{qr})_{1,j} D_0^r v_{1,j} \right]. \end{aligned} \quad (3.12)$$

The factor within the square brackets is identical to the boundary condition (3.7) and therefore vanishes. The second term of (3.11) also vanish due to (3.7) and, finally, the third and fourth terms vanish due to the boundary condition (3.8). This finalizes the proof. \square

A direct consequence of lemma 1 is the following corollary.

Corollary 1 (Conservation of energy). All real-valued solutions (u, v) to the equations (3.3), (3.4) with boundary conditions (3.5), (3.6), (3.7) and (3.8), satisfy

$$\|\sqrt{J\rho}u_t\|_h^2 + \|\sqrt{J\rho}v_t\|_h^2 - (u, L^{(u)}(u, v))_h - (v, L^{(v)}(u, v))_h = C. \quad (3.13)$$

Here C is a constant depending only on the initial data.

Proof. Lemma 1 gives

$$\begin{aligned} \frac{1}{2} \frac{d}{dt} \left(\|\sqrt{J\rho}u_t\|_h^2 + \|\sqrt{J\rho}v_t\|_h^2 \right) = \\ \frac{1}{2} \left((u_t, L^{(u)}(u, v))_h + (v_t, L^{(v)}(u, v))_h + (u, L^{(u)}(u_t, v_t))_h + (v, L^{(v)}(u_t, v_t))_h \right) = \\ \frac{1}{2} \frac{d}{dt} \left((u, L^{(u)}(u, v))_h + (v, L^{(v)}(u, v))_h \right). \end{aligned}$$

By integrating the above expression in time we arrive at (3.13). \square

For the quantity in (3.13) to be an energy we need the following result. Define

$$\begin{aligned}
\mathcal{P}_1 &= \|\sqrt{J\lambda}(q_x \widetilde{D}_0^q u + r_x D_0^r u + q_y \widetilde{D}_0^q v + r_y D_0^r v)\|_h^2 + \|\sqrt{J2\mu}(q_x \widetilde{D}_0^q u + r_x D_0^r u)\|_h^2 \\
&\quad + \|\sqrt{J2\mu}(q_y \widetilde{D}_0^q v + r_y D_0^r v)\|_h^2 + \|\sqrt{J\mu}(q_y \widetilde{D}_0^q u + r_y D_0^r u + q_x \widetilde{D}_0^q v + r_x D_0^r v)\|_{h'}^2, \\
\mathcal{P}_2 &= \frac{h_r^2}{4} \left(\|\sqrt{J2\mu} r_x D_+^r D_-^r u\|_h^2 + \|\sqrt{J2\mu} r_y D_+^r D_-^r v\|_h^2 \right) \\
&\quad + \frac{h_q^2}{4} \left(\|\sqrt{J2\mu} q_x D_+^q D_-^q u\|_{h_\gamma}^2 + \|\sqrt{J2\mu} q_y D_+^q D_-^q v\|_{h_\gamma}^2 \right) \\
&\quad + \frac{h_r^2}{4} \|\sqrt{J\lambda}(r_x D_+^r D_-^r u + r_y D_+^r D_-^r v)\|_h^2 + \frac{h_q^2}{4} \|\sqrt{J\lambda}(q_x D_+^q D_-^q u + q_y D_+^q D_-^q v)\|_{h_\gamma}^2 \\
&\quad + \frac{h_r^2}{4} \|\sqrt{J\mu}(r_x D_+^r D_-^r v + r_y D_+^r D_-^r u)\|_h^2 + \frac{h_q^2}{4} \|\sqrt{J\mu}(q_x D_+^q D_-^q v + q_y D_+^q D_-^q u)\|_{h_\gamma}^2, \\
\mathcal{P}_3 &= \frac{h_r}{2} \sum_{j=1}^{N_r} \left((J\lambda)_{N_{q,j}} ((q_x)_{N_{q,j}} u_{N_{q-1,j}} + (q_y)_{N_{q,j}} v_{N_{q-1,j}})^2 \right. \\
&\quad \left. + (J\mu)_{N_{q,j}} ((q_x)_{N_{q,j}} v_{N_{q-1,j}} + (q_y)_{N_{q,j}} u_{N_{q-1,j}})^2 \right), \\
\mathcal{P}_4 &= \frac{h_q h_r}{2} \sum_{j=1}^{N_r} \left((J\lambda)_{3/2,j} ((q_x)_{3/2,j} D_+^q u_{1,j} + (q_y)_{3/2,j} D_+^q v_{1,j})^2 \right. \\
&\quad \left. + (J\mu)_{3/2,j} ((q_x)_{3/2,j} D_+^q v_{1,j} + (q_y)_{3/2,j} D_+^q u_{1,j})^2 \right. \\
&\quad \left. + (J2\mu)_{3/2,j} ((q_x)_{3/2,j} D_+^q u_{1,j})^2 + ((q_y)_{3/2,j} D_+^q v_{1,j})^2 \right).
\end{aligned}$$

We have

Lemma 2 (Ellipticity). For all real-valued grid functions (u, v) satisfying the discrete boundary conditions (3.5), (3.6), (3.7), (3.8), the spatial operators $L^{(u)}(u, v)$ and $L^{(v)}(u, v)$ satisfy

$$-(u, L^{(u)}(u, v))_h - (v, L^{(v)}(u, v))_h = \mathcal{P}_1 + \mathcal{P}_2 + \mathcal{P}_3 + \mathcal{P}_4, \quad (3.14)$$

where $\mathcal{P}_1 \geq 0, \mathcal{P}_2 \geq 0, \mathcal{P}_3 \geq 0, \mathcal{P}_4 \geq 0$.

Proof. The equality (3.14) is derived by using identities (3.10) together with the following summation by parts rules,

$$\begin{aligned}
(u, D_-^r E_{1/2}^r(\sigma) D_+^r v)_h &= - \underbrace{(D_0^r u, D_0^r v)_h}_{t_1} - \underbrace{\frac{h_r^2}{4} (D_+^r D_-^r u, \sigma D_+^r D_-^r v)_h}_{t_2}, \\
(u, D_-^q E_{1/2}^q(\sigma) D_+^q v)_h &= - \underbrace{(D_0^q u, D_0^q v)_h}_{t_3} - \underbrace{\frac{h_q^2}{4} (D_+^q D_-^q u, \sigma D_+^q D_-^q v)_{h_\gamma}}_{t_4} + h_r \sum_{j=1}^{N_r} (-t_{5j} - t_{6j} + t_{7j} + t_{8j}),
\end{aligned}$$

where

$$\begin{aligned} t_{5j} &= \frac{1}{2} \sigma_{1/2,j} u_{1,j} D_+^q v_{0,j}, & t_{6j} &= \frac{1}{2} \sigma_{3/2,j} u_{2,j} D_+^q v_{1,j}, \\ t_{7j} &= \frac{\sigma_{N_q,j}}{2} u_{N_q-1,j} D_+^q u_{N_q-1,j}, & t_{8j} &= \frac{\sigma_{N_q-1,j}}{2} u_{N_q,j} D_+^q u_{N_q-1,j}. \end{aligned}$$

Here the inner product $(w, v)_{h\gamma}$ is defined as

$$(w, u)_{h\gamma} = h_q h_r \sum_{j=1}^{N_r} \sum_{i=2}^{N_q} w_{i,j} u_{i,j}.$$

The corresponding norm is $\|w\|_{h\gamma}^2 = (w, w)_{h\gamma}$.

To verify (3.14), terms of the type t_1 and t_3 are collected into \mathcal{P}_1 and terms of type t_2 and t_4 into \mathcal{P}_2 . The t_{8j} and one part of the t_{7j} terms vanish due to the homogeneous Dirichlet boundary conditions (3.5), while the remaining contribution from the t_{7j} terms goes into \mathcal{P}_3 . Using $v_{2,j} = v_{1,j} + h_q D_+^q v_{1,j}$ in the t_{6j} term gives the contributions of \mathcal{P}_4 . Collecting all the remaining boundary terms gives an expression identical to (3.12) (with $u^0 = u^1 = u$) and another term identical to the expression corresponding to (3.12) for the second free surface boundary condition (3.8). As the free surface boundary conditions are assumed to hold, the lemma is proved. \square

3.3 Temporal discretization

In time we discretize using second order accurate centered differences. The fully discrete equations are

$$\begin{aligned} u^{n+1} - 2u^n + u^{n-1} &= (\rho J)^{-1} k^2 L^{(u)}(u^n, v^n), \\ v^{n+1} - 2v^n + v^{n-1} &= (\rho J)^{-1} k^2 L^{(v)}(u^n, v^n). \end{aligned} \quad (3.15)$$

For the fully discrete equations it can be shown that the following lemma holds.

Lemma 3.1 (Discrete conservation of energy). *Let $(u, v)_{\rho J}$ be the weighted inner product defined by $(f, (\rho J)^{-1} g)_{\rho J} = (f, g)_h$, and let $C_e(t_{n+1})$ be the discrete energy*

$$\begin{aligned} C_e(t_{n+1}) &= \\ &\|D_+^t u^n\|_{\rho J}^2 + \|D_+^t v^n\|_{\rho J}^2 - (u^{n+1}, (\rho J)^{-1} L^{(u)}(u^n, v^n))_{\rho J} - (v^{n+1}, (\rho J)^{-1} L^{(v)}(u^n, v^n))_{\rho J}. \end{aligned} \quad (3.16)$$

If $u^q, v^q, q = n-1, n, n+1$ are solutions to (3.15) and satisfy the discrete boundary conditions (3.5), (3.6), (3.7), (3.8) then

$$C_e(t_{n+1}) = C_e(t_n).$$

The proof of the lemma is the same as for the Cartesian discretization and can be found in [17] (theorem 3).

3.4 Corners where free surfaces meet

As was stated above, the key ingredient to obtain a stable and explicit discretization of the free surface at Γ_1 is to use the boundary modified difference operator \widetilde{D}_0^q for the normal derivative in the cross derivative terms in the equation. For cases with more than one free surface we use difference operators that are modified at those other free surfaces as well. For example, when the boundary Γ_4 is changed into a free surface and the boundary Γ_2 is changed into a homogeneous Dirichlet boundary, the grid in r is changed to

$$r_j = (j-1)h_r, \quad j=0, \dots, N_r, \quad h_r = 1/(N_r-1).$$

Now the grid indexes $(i,j) \in [1, N_q-1] \times [1, N_r-1]$ belong to interior points. Also, the discretization of the equations is changed by using the modified operator

$$\widetilde{D}_0^r u_{i,j} = \begin{cases} D_+^r u_{i,j}, & j=1, \\ D_0^r u_{i,j}, & j \geq 2, \end{cases}$$

instead of D_0^r . Now, at the point (q_1, r_1) we need to use the free surface boundary conditions on Γ_1 to get the values for $u_{0,1}$ and $v_{0,1}$ and the free surface boundary conditions on Γ_4 to get the values for $u_{1,0}$ and $v_{1,0}$. By repeating the steps in the proofs of the different lemmata it is easy to see that for the self-adjointness and conservation results to hold we have to modify the discretization of the boundary conditions at the corners. Not surprisingly, the correct modification consists of replacing D_0^r by \widetilde{D}_0^r in (3.3) and (3.4) and replacing D_0^q by \widetilde{D}_0^q in the free surface boundary condition discretization along Γ_4 . These modifications, apart from being necessary for stability, are also good from an implementations point of view because all free surface boundaries can be updated independent of each other, keeping the method fully explicit.

When implementing the method in a practical computer code it is important to apply the boundary conditions in the correct order. Given the solution on the two previous time levels t_n and t_{n-1} the steps to advance the solution to time level $n+1$ are the following:

1. Update all Dirichlet b.c. on time level t_n ,
2. Update all periodic b.c. on time level t_n ,
3. Update all free-surface b.c. on time level t_n ,
4. Use equation (3.15) to get the solution at t_{n+1} .

3.4.1 Extension to three dimensions

The extension of the scheme to three dimensions is straightforward. Given a one to one mapping $(x(q,r,s), y(q,r,s), z(q,r,s)), q, r, s \in [0, 1]$, the three dimensional elastic wave equation can be formulated in conservative form in the curvilinear coordinate system. The resulting equations are discretized in the same way as (2.6)-(2.7). Again, if a boundary

has free surface condition, then a modified difference operator is used for the normal derivative in the cross derivative terms in the governing equation. As for the corner case above, at edges between free surfaces the modified difference operators for the *tangential derivatives in the free surface boundary conditions* are used. The same recipe is used for the tangential derivatives in the boundary conditions in three dimensions corners where three free surfaces meet.

Remark 3. It is straightforward (but tedious) to show that lemma 1, 2 and corollary 1 in §3.2 generalize to the three-dimensional case.

4 Numerical examples

In this section we present numerical experiments with the numerical method described above. We start with two verification examples and proceed with four more application oriented examples, illustrating the versatility of the method.

4.1 Verification: Method of manufactured solution in two dimensions

N	maxerr u	maxerr v	$e_i/e_{i+1}, u$	$e_i/e_{i+1}, v$
80	0.16533	0.15609		
160	0.04245	0.03912	3.89	3.99
320	0.01071	0.00971	3.96	4.03
640	0.00269	0.00240	3.98	4.04

Table 1: Experimentally determined order of accuracy using the method of manufactured solution.

A powerful way to verify the correctness of the implementation of any numerical method is the method of manufactured solution. The method works as follows: postulate a smooth solution described by functions that are easy to differentiate. In this example we choose

$$u = \sin(6.2(x - 1.3t))\sin(6.2y), \quad (4.1)$$

$$v = \sin(6.2(x - 1.2t))\sin(6.2y). \quad (4.2)$$

Insert the postulated solution into the governing equations and the boundary conditions to determine the external forcing that would give the desired solution (for example, if the equation was $u_t + u_x = f$, then we would set $f = 6.2(1 - 1.3)\cos(6.2(x - 1.3t))\sin(6.2y)$ in order to manufacture the solution (4.1)).

The computational domain we consider is defined by the mapping

$$x = q + 0.05\sin(\pi(r - 0.5)), \quad y = r + 0.05\sin(\pi(q - 0.5)), \quad (q, r) \in [0, 1]^2.$$

On the surfaces corresponding to $q = 0$ and $r = 0$ free surface boundary conditions are imposed and on the surfaces $q = 1$ and $r = 1$ Dirichlet boundary conditions are imposed. We choose the Lamé parameters to be $\lambda = \mu = 1$ and advanced the solution up to time $\pi/5$ with a time step $k = 0.1h$, where, $h_r = h_q = h = \pi/N$, $N = 80, 160, 320, 640$. At the final time the maximum error is computed and tabulated in Table 1. From the results we conjecture that the method is second order accurate.

4.2 Verification: Conservation of discrete energy in three dimensions

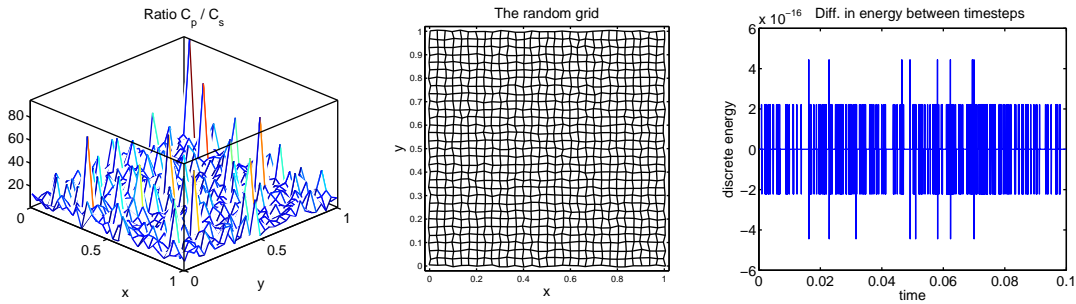


Figure 2: To the left: Ratio of the randomly chosen P and S - wave velocities on the free surface $s=0$. In the middle: The grid on the free surface $s=0$. The grid is made up of a regular Cartesian grid whose grid-points has been randomly perturbed. To the right: The difference in the (3-D version) discrete energy (3.16) of subsequent time steps. The discrete energy is conserved to machine precision.

The fact that the scheme conserves a discrete energy can be used as another tool to verify the correctness of the code. The idea is to use random (but physically valid $\rho, \lambda, \mu > 0$) data for the initial values, the material parameters and for the grid (we require $J > 0$).

The grid is constructed by first discretizing the 3-D unit cube with a grid spacing of $1/40$, then the x, y, z coordinates of all regular grid points are perturbed by a uniformly distributed random variable taking values in $[-0.005, 0.005]$. A plot of the first vertical grid plane (corresponding to $s=0$) projected onto the x - y plane can be found in Figure 2. The Lamé parameters are given by

$$\lambda(x, y, z) = 1 + R_{10000}, \quad \mu(x, y, z) = 1 + R_{100},$$

where R_p is a uniformly distributed random variable taking values in $[0, p]$. A plot of the point-wise ratio between C_p and C_s can be found in Figure 2. The initial data is prescribed as uniformly distributed random variables, with a magnitude chosen such that the initial discrete energy is of order one. Free-surface boundary conditions are imposed on the top and bottom of the cube and homogeneous Dirichlet conditions are imposed on the rest of the faces. The solution is advanced up to time 0.1. To the right in Figure 2 the difference in discrete energy between subsequent time steps is plotted. As can be seen the size of the difference is at machine precision, thus verifying the correctness of the implementation and the conservation properties of the method.

4.3 Effects of curvature in a thin wave guide

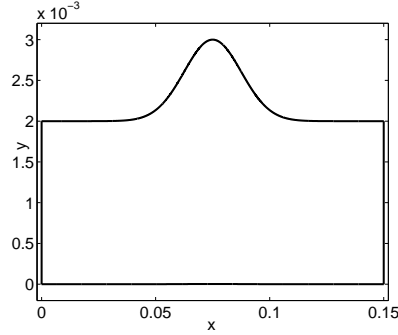


Figure 3: The thin wave guide with a small perturbation on the upper side. Note that the scaling of the axes are very different. The units are given in meter.

It is known that the properties of surface waves in solids depend on both the curvature and the polarization of the displacement field [3]. For certain polarizations and curvature the group and/or phase velocities of the surface waves increase and for other they decrease. These features can be used in nondestructive testing applications to, for example, determine the effect of change in cross section of free surface wave-guides, see [16].

In this example we consider a problem setup, inspired by the experiments in [16], consisting of a thin long aluminum wave guide with a slowly varying cross section, see Figure 3. The material properties of the wave guide are $\lambda = 70\text{GPa}$, $\mu = 35\text{GPa}$, $\rho = 2700\text{kg}/\text{m}^3$. The guide is 150mm long and at the ends it is 2mm wide. The upper surface of the wave guide is described by the equation

$$y(x) = 2 + e^{-0.003203(x-75)^2},$$

where x and y are given in mm . The rightmost part of the wave guide is clamped and the other three sides are free.

We are interested in how small wave packages, mainly confined to the free surface, are affected by the curvature. To create such wave packages we add a time dependent forcing to the left free surface boundary. Precisely, we take the boundary conditions to be

$$\begin{bmatrix} (2\mu + \lambda)u_x + \lambda v_y & \mu(v_x + u_y) \\ \mu(v_x + u_y) & (2\mu + \lambda)v_y + \lambda u_x \end{bmatrix} \begin{bmatrix} n_x \\ n_y \end{bmatrix} = \begin{bmatrix} 0 \\ 5 \cdot 10^8 g(t) \end{bmatrix} \quad (4.3)$$

were

$$g(t) = \sin(2\pi f t) e^{-\left(\frac{t-t_0}{\delta}\right)^2}, \quad f = 5.0\text{MHz}, \quad t_0 = 2\mu\text{s}, \quad \delta = 0.5\mu\text{s}.$$

The wave-guide is discretized using a grid consisting of 7502×103 points. Towards the ends of the grid each cell is approximately a square with side $\sim 20\mu\text{m}$ while at the

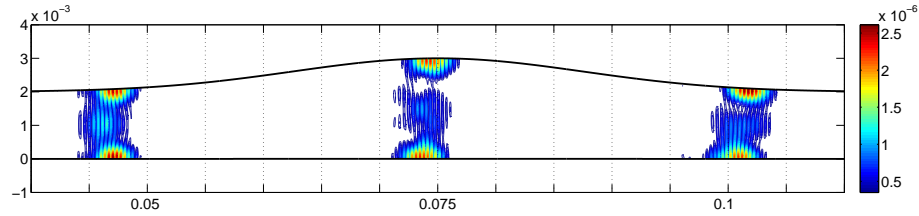


Figure 4: Magnitude of the solution at three time instants, $t = 15.9\mu s$, $23.8\mu s$, $31.8\mu s$. The upper wave package is accelerated as it passes the curved section and arrives first to the clamped boundary to the right.

bump the cells are slightly rectangular with a shortest side in the x direction of $20\mu m$. For the waves induced by the boundary condition (4.3) this discretization gives a resolution of approximately 20 points per wavelength.

The simulation runs up to time $t = 35\mu s$. In Figure 4 an overlay contour plot of the magnitude of the solution at times $t = 15.9\mu s$, $23.8\mu s$, $31.8\mu s$ illustrates how the solution propagates from left to right. Initially the wave packages, on the upper and lower boundary, travel with the same speed but as the wave guide expands, the wave package along the curved boundary accelerates and moves ahead of the package at the flat boundary. For a close up of the magnitude of the solution along the boundaries, see Figure 5.

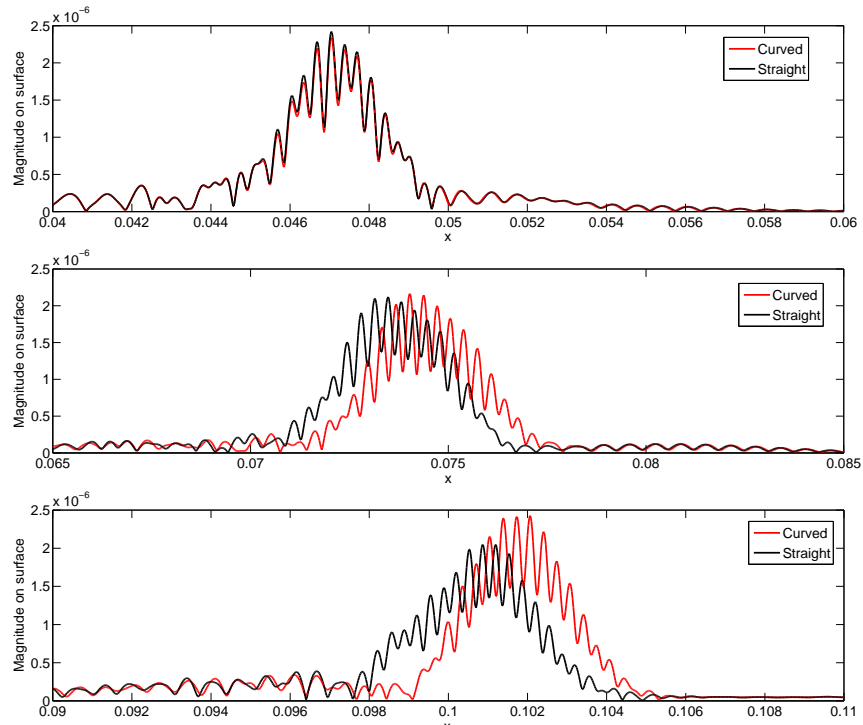


Figure 5: From top to bottom: Magnitude of the solution along the top (Curved) and the bottom (Straight) boundaries at time $15.9\mu s$, $23.8\mu s$ and $31.8\mu s$. Note that the horizontal axis are different in the different plots.

This experiment illustrates that, even for small changes in curvature, accurate representation of the geometry is crucial for obtaining the correct results.

4.4 Effects of topography in two dimensions

Curved surfaces, or rather topography, can have significant effects on the ground motions after a seismic event. To illustrate this we solve a variation of Lamb's problem on a domain with a simple topographical feature. The computational domain is composed of a "halfspace" $x \in [-20, 20]$ km and $y \in [0, -20]$ km. In the left part of the halfspace there is a small mountain (see Figure 6) whose elevation (in kilometers) is described by the equation

$$y(x) = 0.2 \exp\left(-\left(\frac{x-15.0}{0.3}\right)^2\right).$$

To focus our study on the effects of boundary curvature the halfspace is assumed to consist of a homogeneous material with P-wave velocity $C_p = 3.2$ km/s, S-wave velocity $C_s = 1.8475$ km/s and density $\rho = 2200.0$ kg/m³.

Initially, the displacements and velocities are zero and the problem is forced by adding the following source term to the free surface boundary conditions

$$\begin{bmatrix} (2\mu + \lambda)u_x + \lambda v_y & \mu(v_x + u_y) \\ \mu(v_x + u_y) & (2\mu + \lambda)v_y + \lambda u_x \end{bmatrix} \begin{bmatrix} n_x \\ n_y \end{bmatrix} = \delta(x)\delta(y)g(t) \begin{bmatrix} n_x \\ n_y \end{bmatrix},$$

where the time dependence is given by a Ricker wavelet

$$g(t) = 10^{13} [2(\pi f_0(t-t_0))^2 - 1] e^{-[\pi f_0(t-t_0)]^2},$$

with $t_0 = 1$ s and $f_0 = 2$ Hz. The domain is discretized with 2001×1001 points and the solution is advanced using a time step $k = 0.004329$ s for ten seconds. The results of the simulations can be found in Figure 6. The small mountain in the left part of the halfspace acts as a scatterer, creating a new family of backscattered P, S and Rayleigh waves. The amplitude of the reflected Rayleigh wave is quite substantial and clearly illustrates the importance of topography.

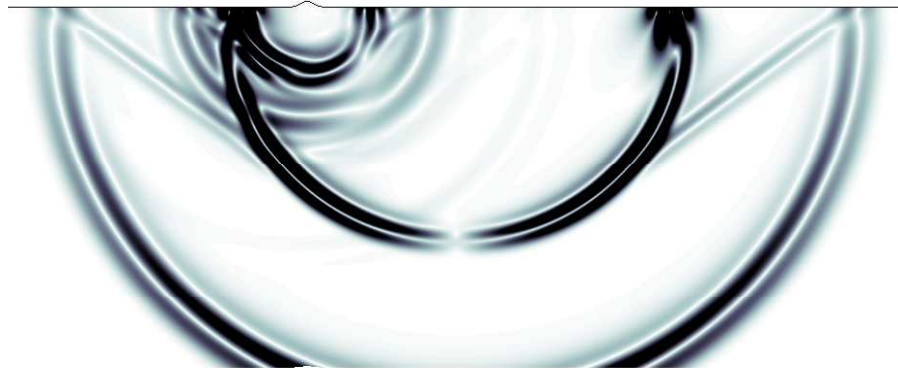
4.5 Effects of topography in three dimensions

As a first three-dimensional problem we consider an example from [13] ("amplification of a three-dimensional hill") with a three-dimensional topography. The topography is described by the hill

$$z(x, y) = 180 \exp\left(-\left(\frac{x-1040}{500}\right)^2 - \left(\frac{y-1040}{250}\right)^2\right) m, \quad (x, y) \in [0m, 2080m]^2.$$



(a) Magnitude at time 2.5974s



(b) Magnitude at time 5.1948s



(c) Magnitude at time 7.7922s

Figure 6: Magnitude of the displacement at different time instants for the variation of Lamb's problem described in §4.4. The color scale is the same in all of the three frames. The small mountain on the left side of the free surface acts as a scatterer, creating a new family of backscattered P,S, von Schmidt and Rayleigh waves.

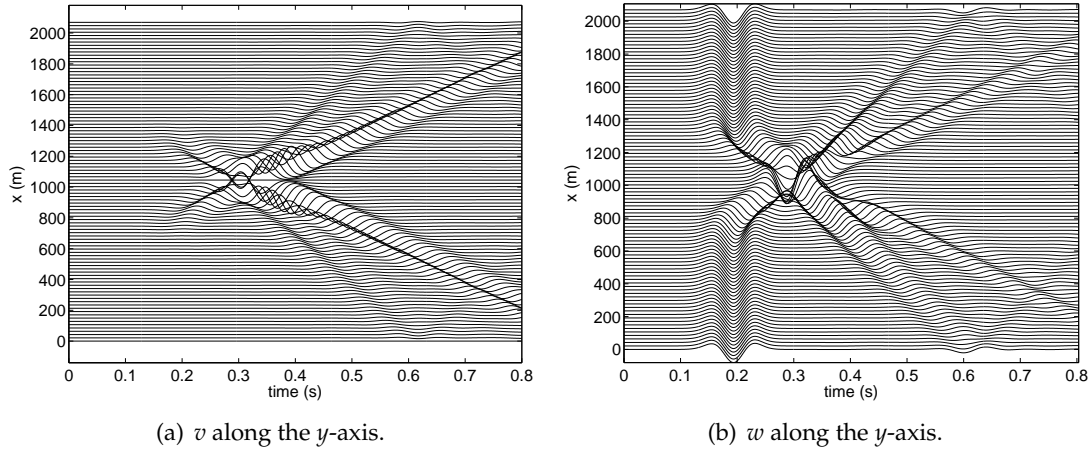


Figure 7: Time responses of the v and w components of the displacement.

The computational domain extends to depth $z(x,y) = -1050m$. The medium is homogeneous with $V_p = 3200m/s$, $V_s = 1847.5m/s$ and $\rho = 2200kg/m^{-3}$. Dirichlet conditions are prescribed for u, v and w on the bottom:

$$\begin{aligned} u(x,y,-1050,t) &= 0, & w(x,y,-1050,t) &= 0, \\ v(x,y,-1050,t) &= 0.5(2(10.2\pi(t-0.5))^2 - 1)e^{-(10.2\pi(t-0.5))^2}. \end{aligned}$$

On the top surface a free surface boundary condition is imposed and periodic conditions are imposed on the other boundaries.

As in [13] the surface displacements are measured along the minor axis (in the y direction). The domain is discretized with 602 grid points in the q and r directions and with 303 points in the s direction. In Figure 7 the time responses of the v and w components are found. As can be seen they agree well with the results depicted in Figure 12 in [13].

4.6 Wave propagation in a thin toroidal shell

As a final example we consider the propagation of waves in a thin toroidal shell with free surfaces. The toroidal shell is described by the mapping

$$\begin{aligned} x(q,r,s) &= (R_1 + (R_2 + s\Delta_R)\cos(2\pi r))\cos(2\pi q), \\ y(q,r,s) &= (R_1 + (R_2 + s\Delta_R)\cos(2\pi r))\sin(2\pi q), \\ z(q,r,s) &= (R_2 + s\Delta_R)\sin(2\pi r), \end{aligned} \tag{4.4}$$

where the larger radius is $R_1 = 4$, the smaller radius is $R_2 = 1$ and the width of the shell is $\Delta_R = 0.1$. The shell consists of a (non-dimensionalized) homogeneous material with $\mu = 1$, $\lambda = 14$ and density $\rho = 1$, i.e. $C_p = 4$ and $C_s = 1$.

At time zero the shell is at rest and to induce waves we introduce a forcing in the free surface boundary condition at the interior shell. That is, at $s=0$, we impose the boundary condition

$$\begin{bmatrix} 2\mu u_x + \lambda \operatorname{div}(\mathbf{u}) & \mu(v_x + u_y) & \mu(w_x + u_z) \\ \mu(v_x + u_y) & 2\mu v_y + \lambda \operatorname{div}(\mathbf{u}) & \mu(w_y + v_z) \\ \mu(w_x + u_z) & \mu(w_y + v_z) & 2\mu w_z + \lambda \operatorname{div}(\mathbf{u}) \end{bmatrix} \begin{bmatrix} n_x \\ n_y \\ n_z \end{bmatrix} = \begin{bmatrix} f \\ 0 \\ 0 \end{bmatrix}, \quad (4.5)$$

were $\operatorname{div}(\mathbf{u}) = u_x + v_y + w_z$, and a point force is applied with a Ricker wavelet time dependence according to

$$f = \delta(x - x_0)\delta(y)\delta(z)10000[2(4\pi(t-1))^2 - 1]e^{-[4\pi(t-1)]^2},$$

and $x_0 = R_1 + R_2$. Note that the above boundary conditions are stated in Cartesian coordinates (for brevity); in the code we obviously discretize the curvilinear version of (4.5).

Since the shell is very thin compared to its circumference it is a fairly challenging task to solve this problem. To get a grid with reasonably uniform cells the shell is discretized with 5081 points in the q -direction, 1315 points in the r -direction and 21 points in the s -direction. Including ghost points, the total number of grid points amount to about 154 million. With this discretization the solution is advanced up to time 20 using a time step $k = 0.0008135$. At various times, snapshots of the solution on the upper half ($r \in [0, 0.5]$) of the inner shell are saved. Some of these snapshots can be found in Figure 8. As can be seen already in subfigure (a), there are a lot of waves that bounce between the free surfaces of the thin shell, generating complicated wave patterns. In the middle of the picture there is a set of smaller wavefronts of faster waves, and further to the right there is a stronger more concentrated wave front of slowly moving waves. At time ~ 8 (subfigure (b)) the wave pattern is dominated by the waves with short wave length, the thin wave to the right has revolved a lap around the shell and is moving to the left. In the next frame (c) the rightmost wave has emerged from the left and is moving to the right. Further to the left, most of waves are concentrated to the outermost part of the shell. Finally, in subfigure (d) the primary wavefront has just focused in the left part of the torus and is now composed of small localized wave crests.

To get a rough understanding of how well the waves are resolved we plot the solution along the line $A-B$ (see Figure 8 (d)). The different components of the displacements are plotted as a functions of the angle in Figure 9 (a). In subfigure (b) a closeup of the displacements close to the most rapidly varying part of the solution are plotted. Each marker represent a grid point and as we can see the waves are fairly well resolved.

5 Summary and discussion

A stable and explicit second order accurate finite difference method for the elastic wave equation in curvilinear coordinates has been presented. The discretization of the spatial

operators in the method has been shown to be selfadjoint for free-surface, Dirichlet and periodic boundary conditions. The fully discrete version of the method has been shown to conserve a discrete energy to machine precision.

It would be of great interest to develop a higher (4th or more) order self-adjoint discretization of the elastic wave equation. The possibilities of using summation by parts techniques to extend the present method to such a high order discretization is currently under investigation.

The curvilinear formulation of the elastic wave equation contains many more terms than the Cartesian formulation, making the present method more expensive than a method on a Cartesian grid. A way to increase the efficiency is to use an overlapping grid approach (see e.g. [5]) where the equations close to curved boundaries are solved on body fitted curvilinear grids while the equations in the interior are solved on Cartesian grids and communication between grids is handled via interpolation. Solving the equations using an overlapping grid approach also enables simulations on domains which (due to singular mappings) cannot be described by a single curvilinear grid (for example a sphere).

Acknowledgments

The authors would like to thank Björn Sjögreen and William Henshaw for stimulating discussions. This work performed under the auspices of the U.S. Department of Energy by Lawrence Livermore National Laboratory under Contract DE-AC52-07NA27344.

References

- [1] Z. Alterman and F. C. Karal. Propagation of elastic waves in layered media by finite difference methods. *Bulletin of the Seismological Society of America*, 58(1):367–398, 1968.
- [2] Z. Alterman and A. Rotenberg. Seismic waves in a quarter plane. *Bulletin of the Seismological Society of America*, 59(1):347–368, 1969.
- [3] L.M. Brekhovskikh. Surface waves confined to the curvature of the boundary in solids. *Soviet Physics - Acoustics*, 13(4):462–472, 1968.
- [4] D. L. Brown. A note on the numerical solution of the wave equation with piecewise smooth coefficients. *Mathematics of Computations*, 42(166):369–391, 1984.
- [5] G. Chesshire and W. Henshaw. Composite overlapping meshes for the solution of partial differential equations. *Journal of Computational Physics*, 90, 1990.
- [6] G. C. Cohen. *Higher-Order Numerical Methods for Transient Wave Equations*. Springer, 2002.
- [7] E. Faccioli, F. Maggio, R. Paolucci, and A. Quarteroni. 2d and 3d elastic wave propagation by a pseudo-spectral domain decomposition method. *Journal of Seismology*, 1(3):237–251, 1997.
- [8] K-A. Feng, C-H. Teng, and M-H. Chen. A pseudospectral penalty scheme for 2d isotropic elastic wave computations. *Journal of Scientific Computing*, 33(3):313–348, 2007.
- [9] B. Fornberg. The pseudospectral method: Comparisons with finite differences for the elastic wave equation. *Geophysics*, 52(4):483–501, 1987.
- [10] A. Ilan and D. Loewenthal. Instability of finite difference schemes due to boundary conditions in elastic media. *Geophysical Prospecting*, 24, 1976.

- [11] Almogha Ilan. Stability of finite difference schemes for the problem of elastic wave propagation in a quarter plane. *Journal of Computational Physics*, 29, 1978.
- [12] M. Käser and M. Dumbser. An arbitrary high-order discontinuous galerkin method for elastic waves on unstructured meshes - i. the two-dimensional isotropic case with external source terms. *Geophysical Journal International*, 166(2):855–877, 2006.
- [13] D. Komatitsch and J.-P. Vilotte. The spectral element method; an efficient tool to simulate the seismic response of 2d and 3d geological structures. *Bulletin of the Seismological Society of America*, 88(2):368–392, 1998.
- [14] H.-O. Kreiss and J. Olinger. Comparison of accurate methods for the integration of hyperbolic equations. *Tellus*, 24:199–215, 1972.
- [15] B. Lombard, J. Piraux, C. Gelis, and J. Virieux. Free and smooth boundaries in 2-d finite-difference schemes for transient elastic waves. *Geophysical Journal International*, 172(1):252–261, 2008.
- [16] P. Marical, M. Ech-Cherif El-Kettani, and M.V. Predoi. Guided waves in elastic plates with gaussian section variation: Experimental and numerical results. *Ultrasonics*, 47(1-4):1–9, 2007.
- [17] S. Nilsson, N. A. Petersson, B. Sjögreen, and H.-O. Kreiss. Stable difference approximations for the elastic wave equation in second order formulation. *SIAM Journal on Numerical Analysis*, 45(5):1902–1936, 2007.
- [18] Stacey R. New finite-difference methods for free surfaces with a stability analysis. *Bulletin of the Seismological Society of America*, 84(1):171–184, 1994.
- [19] J. F. Thompson, Z. U.A. Warsi, and C. W. Mastin. *Numerical grid generation: foundations and applications*. Elsevier North-Holland, Inc., New York, NY, USA, 1985.
- [20] Jeroen Tromp, Dimitri Komatitsch, and Qinya Liu. Spectral-element and adjoint methods in seismology. *Commun. Comput. Phys.*, 3(1–32), 2008.
- [21] J. E. Vidale and R. W. Clayton. A stable free-surface boundary condition for two-dimensional elastic finite-difference wave simulation. *Geophysics*, 51, 1986.
- [22] W. Zhang and X. Chen. Traction image method for irregular free surface boundaries in finite difference seismic wave simulation. *Geophysical Journal International*, 167(1):337–353, 2006.

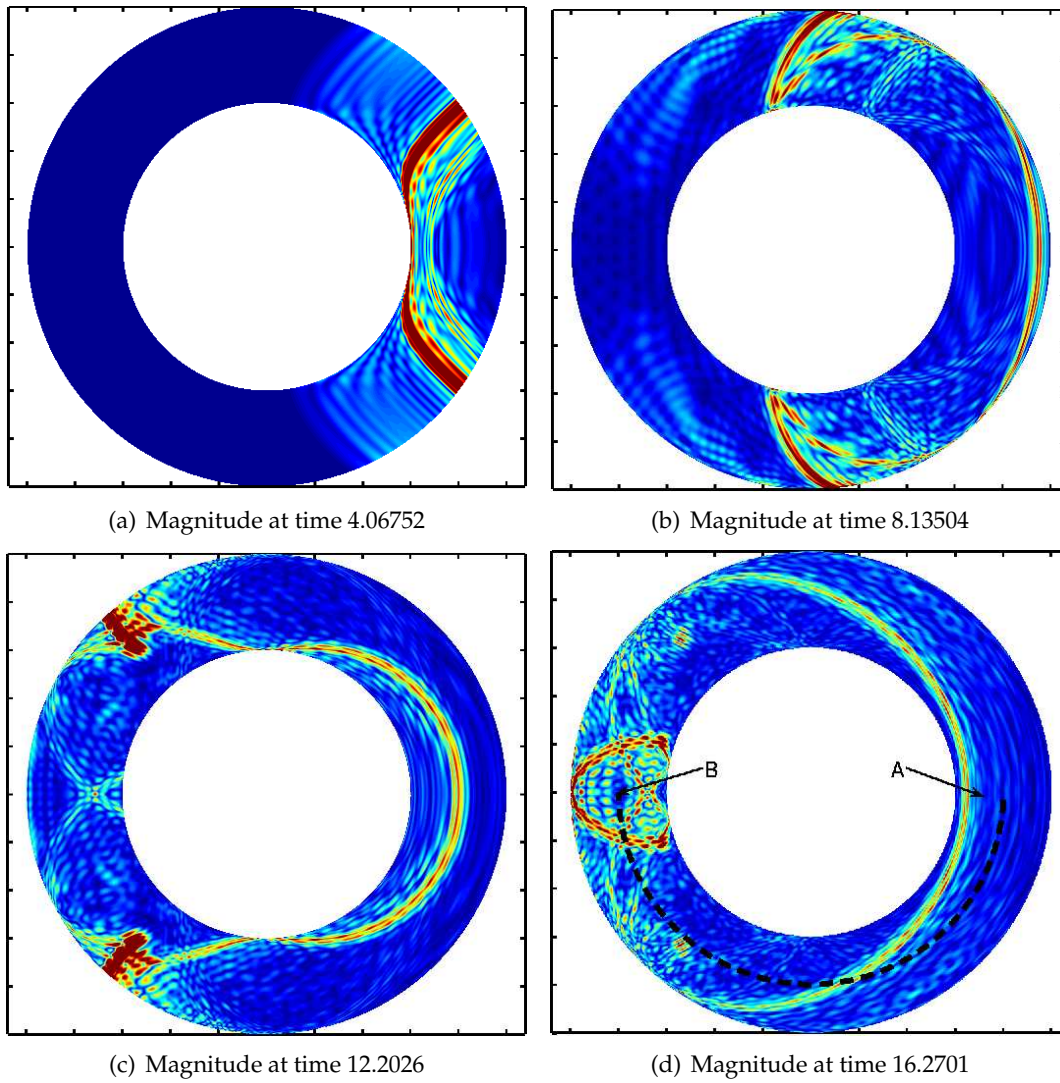
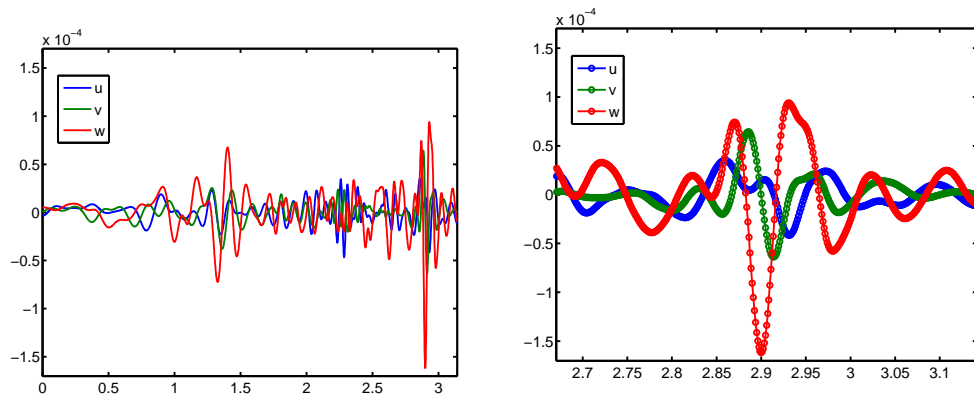


Figure 8: The magnitude of the wave field at different times on the upper half of the inner surface in the three dimensional toroidal shell described by the mapping (4.4).



(a) The solution along the centerline $A-B$ (see Figure 8 (d)).
 (b) Zoom in on the most oscillatory part, each marker represent a grid point. Even the steepest waves are fairly well resolved.

Figure 9: The solution along the line $A-B$ (see Figure 8 (d)) at time 16.2701.